

A liquid crystal atmospheric turbulence simulator

Lifa Hu, Li Xuan, Zhaoliang Cao, Quanquan Mu, Dayu Li and Yonggang Liu

State key laboratory of applied optics, Changchun institute of optics, fine mechanics and physics, Chinese Academy of Science, Changchun 130033, China
hulifa@ciomp.ac.cn

Abstract: In the paper, a method to calculate the time evolution turbulence wavefronts based on the covariance method is theoretically presented in detail. According to it, the time-evolution wavefronts disturbed by atmospheric turbulence were experimentally generated by our LC atmospheric turbulence simulator (ATS) based on liquid crystal on silicon (LCOS) with high pixel density, and measured with a wavefront sensor. The advantage of such a LC ATS over a conventional one is that it is flexible with considering the weather parameters of wind speed and C_n^2 , and is relatively easy to control.

©2006 Optical Society of America

OCIS codes: (230.6120) spatial light modulators; (010.1330) atmospheric turbulence; (160.3710) liquid crystals; (010.1080) adaptive optics.

References and Links

1. K. J. Gamble, A. R. Weeks, H. R. Myler, and W. A. Rabadi, "Results of two-dimensional time-evolved phase screen computer simulations," in *Atmospheric Propagation and Remote Sensing IV*, J. Christopher Dainty, ed., Proc. SPIE **2471**, 170-180 (1995).
2. T.-L. Kelly, D. F. Buscher, P. Clark, C. Dunlop, G. Love, R. M. Myers, R. Sharples, and A. Zadrozny, "Dual-conjugate wavefront generation for adaptive optics," *Opt. Express* **17**, 368-374 (2000).
3. T. S. Taylor and D. A. Gregory, "Laboratory simulation of atmospheric turbulence-induced optical wavefront distortion," *Opt. Laser Technol.* **34**, 665-669 (2002).
4. S. Thomas, "A simple turbulence simulator for adaptive optics," in *Advancements in Adaptive Optics*, D. B. Calia, B. L. Ellerbroek, R. Ragazzoni, eds., Proc. SPIE **5490**, 766-773 (2004).
5. M. K. Giles, A. Seward, M. A. Vorontsov, J. Rha, and R. Jimenez, "Setting up a liquid crystal phase screen to simulate atmospheric turbulence," in *High-Resolution Wavefront Control: Methods, Devices, and Applications II*, J. D. Gonglewski, M. A. Vorontsov, M. T. Gruneisen, eds., Proc. SPIE **4124**, 89-97 (2000).
6. M. A. A. Neil, M. J. Booth, and T. Wilson, "Dynamic wave-front generation for the characterization and testing of optical systems," *Opt. Lett.* **23**, 1849-1851 (1998).
7. D. J. Cho, S. T. Thdurman, J. T. Donner, and G. M. Morris, "Characteristics of a 128×128 liquid-crystal spatial light modulator for wave-front generation," *Opt. Lett.* **23**, 969-971 (1998).
8. R. J. Noll, "Zernike polynomials and atmospheric turbulence," *J. Opt. Soc. Am.* **66**, 207-211 (1976).
9. N. Roddier, "Atmospheric wavefront simulation using Zernike polynomials," *Opt. Eng.* **29**, 1174-1180 (1990).
10. M. C. Roggemann, B. M. Welsh, D. Montera, and T. A. Rhoadarmer, "Method for simulating atmospheric turbulence phase effects for multiple time slices and anisoplanatic conditions," *Appl. Opt.* **34**, 4037-4051 (1995).
11. F. Roddier, *Adaptive optics in astronomy*, (Cambridge, Cambridge University Press, 1999), pp. 9-56.

1. Introduction

Both the astronomical observation and the laser communication are closely related to the turbulent atmosphere. The turbulent atmosphere causes a fluctuation of the phase of the wavefront passing through it, which has a strong effect on the quality of astronomical images and the laser shape. To design and evaluate the setups for the astronomy observation and laser communications, different kinds of atmospheric turbulence simulator (ATS) were developed to simulate the effect that atmosphere turbulence has on optical beams in a controllable way [1-4]. One is based on the glass phase screen that has an uneven surface. One rotates it to

generate the time-varying wavefront aberrations. Its main drawbacks are the unchangeable surface and periodicity. The other is a liquid crystal atmospheric turbulence simulator (LC ATS) in which a liquid crystal spatial light modulator (LC SLM) is used to generate wavefronts with the correct spatial and temporal statistics [5-7]. Compared with static phase plates (near-index matching or holographic) or heated air or fluid, LCOS based LC ATS could produce dynamic turbulence wavefront. In addition, unlike phase wheels that give a set limited periodic wavefront, the LC ATS could provide an infinite sequence of time evolved wavefront, and is easily reprogrammable. It has merits of low cost, low power loss, compact, small volume, and no mechanical movement.

Most efforts were made to find approaches to generate atmospheric wavefront with the correct statistics and the time evolution. They are mainly based on Fourier transformation and Zernike covariance [8-10]. The main drawback of the first method is that some aberrations, such as tilt, are underestimated due to low frequency inadequate sampling. Since tilt is the main aberrations of the atmospheric wavefront, the simulated wavefront based on the Fourier transformation will have big statistical errors. Instead, the method of Zernike covariance has correct statistics without the problem of low frequency inadequate sampling. Therefore, in the paper, we will use the method to generate the atmospheric wavefront. Zernike covariance method was presented by R. J. Noll in 1976 [8], and specified theoretically by N. Roddier in 1990 [9]. In fact, they only generate atmospheric wavefronts with the correct spatial statistics. But, it is also necessary for the wavefronts to have a correct time statistics, that is, to generate time-evolution wavefronts. Secondly, some applications, such as astronomical imaging and laser communication, make it important for ATS to generate wavefronts according to given atmospheric and optical system conditions. Therefore, the theoretical method should also include parameters, such as wind speed, altitude and refractive index structure constant and so on. Additionally, the execution time for each random wavefront is long especially for thousands of Zernike modes. Shortening the execution time will make the LC ATS valuable and practicable. Finally, available LC ATS did not take into account some factors, such as the aberrations of the LC screen and regular pixel's diffraction and so on, which leads to apparent errors between measured and theoretical results.

In the paper, we demonstrate a programmable LC ATS based on Kolmogorov theory with the Zernike covariance method. A reflective LC screen based on the liquid crystal on silicon (LCOS) was used. Some factors about the LC screen were taken into account to decrease the turbulence simulation error. Then, a simulation software LC Turb based on Visual C++ and Matlab language was programmed to control the LC ATS. Finally, the time-evolution wavefronts disturbed by atmospheric turbulence generated by our LC ATS were experimentally measured with a wavefront sensor of HASO 32 of Imagine optics.

2. Generation of dynamic turbulence wavefronts

We should briefly summarize the Zernike covariance method presented in Refs. [8] and [9]. We model the wavefront disturbance to match Kolmogorov turbulence statistics. And the Phase screens are generated on a unit circle using a weighted sum of Zernikes. And Zernike polynomials are defined in Ref. [8]. It is not possible to simulate directly a wavefront by obtaining these Zernike coefficients because there is a given covariance E between them due to the fact that the Zernike polynomials are not statistically independent. The independent random Karhunen-Loève coefficients can be computed, then, converted to Zernike coefficients according to the Karhunen-Loève Zernike expansion [9]. Finally, the turbulence wavefronts could be generated from the obtained Zernike coefficients.

For LC ATS's repeatable and reliable laboratory applications in the adaptive optics instrumentation, we did the following works. First, to improve the calculation speed and achieve desired precision, it is necessary to optimize the Zernike mode number N and grid number. The Zernike mode number N should be chosen so that the index of the generated turbulence phase structure function is close to $5/3$. In addition, the residual errors (Δ_N) of turbulence phase simulation for large N could be calculated as:

$$\Delta_N = 0.2944N^{-\sqrt{3}/2}(R_z/r_0)^{5/3} \quad (\text{rad}^2) \quad (1)$$

The correspondent rms value is equal to $\Delta_N^{1/2}$. For different scaling factors (R_z/r_0), R_z is the diameter of simulated area, the rms as a function of N is shown in Fig. 1 for wavelength λ of 632.8nm. For example, it could be seen that rms will be 0.07λ for scaling factor of 10 and N of 120. Larger R_z/r_0 will lead to larger N to obtain the same rms values of 0.07λ . In addition, because the target error should be smaller than 0.07λ , for lab testing of AO systems, this limit would bias the results toward better performance since it would leave out higher spatial frequency components. The calculation speed should be improved and decrease the rms for a real-time calculation of turbulence wavefronts. If the real-time calculation is not possible, another way is to calculate a series of turbulence wavefronts before testing an AO system, and save them to BMP files. Finally display these BMP files orderly on LCOS when testing an AO system.

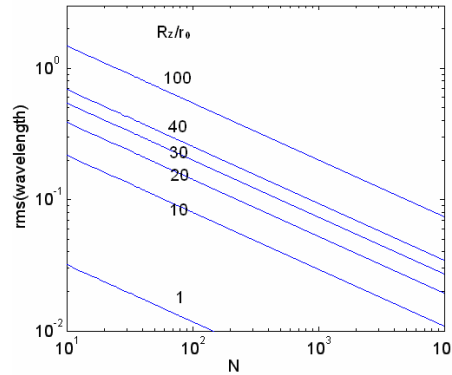


Fig. 1. rms as a function of number of Zernike modes N for different scaling factor R_z/r_0

Secondly, we will not simply define the scaling factor (R_z/r_0) as a constant without taking into account parameters, such as altitude h , zenith angle β and wind speed. We could calculate r_0 with the real-world parameters to generate the turbulence phase. And r_0 is widely used to characterize the level of turbulence at a particular site and could be calculated as [11]:

$$r_0 = \left[0.423 \left(\frac{2\pi}{\lambda} \right)^2 \sec \beta \int_{path} C_n^2(h) dh \right]^{-3/5} \quad (2)$$

Where, λ is wavelength, β is the zenith angle. Its value varies from a few meters in very good seeing conditions to a few centimeters in difficult seeing at visible wavelengths. C_n^2 , named as the index structure coefficient, is a measure of the strength of turbulence. Its value ranges from $10^{-14} \text{ m}^{-2/3}$ to $10^{-18} \text{ m}^{-2/3}$. Usually, Hufnagel-Valley Boundary model is often used to predict the C_n^2 profiles:

$$C_n^2(h) = 5.94 \times 10^{-23} h^{10} e^{-h(v/27)} + 2.7 \times 10^{-16} e^{-2h/3} + C_n^2(0) e^{-10h} \quad (3)$$

Where, h is the altitude in kilometers, v is the wind speed in m/s. And $C_n^2(0)$ is the index structure coefficient at ground boundary layer. It will be more intuitionistic and valuable for a laboratory turbulence simulation. In the paper, we used the Hufnagel-Valley Boundary model. In fact, it is also possible to use other proper models or practical measured data of C_n^2 as a function of altitude and wind speed.

Thirdly, the time-evolution turbulence wavefronts could not be obtained just by changing the Zernike coefficients because the produced random Zernike coefficients at different times

lead to random wavefronts. But we could use the well-known Taylor hypothesis, that is, to produce a large-size wavefront and make it fluently move through the light according to the wind speed and direction. In fact, the produced wavefront is defined on a normalized unit circle. What's more, the Zernike covariance was obtained with Wiener Power spectrum assuming that the inner scale l_0 is zero and the outer scale L_0 is infinity. Therefore, it is reasonable to define a radius R_z of the produced wavefront. R_z should be large enough and smaller than L_0 , so as to generate turbulence wavefront and decrease its periodic phenomenon as possible.

To generate dynamic turbulence, the schematic diagram is shown in Fig. 2. If one does not take into account the direction of wind, it is reasonable to define the moving route as a circle along route A in Fig. 2. If the moving direction is chosen as same as that of wind, linear route as route B is reasonable. In the paper, route B is selected. After the moving route is defined, the duration of time for simulation will be equal to L/v , where L is the length of the chosen route. The time step ΔT should be chosen reasonably so that the simulated turbulence seems fluent. It should be noted that L_A and L_B are the length of route A and B, respectively. First, we calculate a large wavefront ϕ_{total} on the area with diameter of R_z . Second, a part wavefront ϕ_1 of ϕ_{total} on the rectangle sub-area with size of $1.33D \times D$ was read, interpolated with available interpolating program and converted to gray map on LCOS with grid of 1024×768 . It should be noted that D is the diameter of an optical system, such as a telescope. In the paper, D is defined as 1m. Third, next wavefront ϕ_2 with the same size was read from the calculated wavefront at a distance away from the first one. The distance could be obtained with wind speed v multiplied by spacing time ΔT . Repeat the third step to generate followed wavefronts. Therefore, we could simulate a dynamic turbulence with our LC ATS.

The parameters for simulation are summarized in table 1. The minimum grid number of a unit circle is proportional to $(R_z/r_0)^2$. For a LC device, the phase wrapping level is 8 at least for a high diffraction efficient. Therefore, the grid number is at least equal to $64(R_z/r_0)^2$ so as to generate turbulence wavefront with enough spatial frequency. In addition, actual optical system size D must be smaller than R_z . The area with the diameter of D is corresponding to an inscribed circle on LCOS. Considering that the aspect ratio of LCOS is about 1.3, we set the grid is $11(D/r_0) \times 8(D/r_0)$. Then, the phase grid is interpolated to for the LCOS.

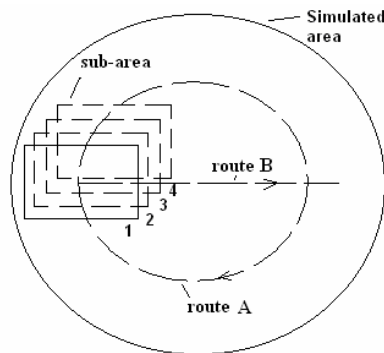


Fig. 2. The schematic diagram of generating dynamic wavefronts.

Table 1. Calculation parameters for turbulence simulation

Parameters	Values
Simulated area	$R_z \times R_z \text{ m}^2$
# of grid samples across simulated area (horiz/vert)	$8(R_z/r_0) \times 8(R_z/r_0)$
Sub-area	$1.3D \times D \text{ m}^2$
# of grid samples across sub-area (horiz/vert)	$11(D/r_0) \times 8(D/r_0)$
Pixels on LCOS(horiz/vert)	1024×768
Size of LCOS(horiz/vert)	$19.5 \times 14.6 \text{ mm}^2$
Duration of simulation	L_A/v (or L_B/v)

3. LC screen and experiment

We use LCR-2500 from Holoeye Inc. in our experiment. Some specifications are listed in Table 2. To produce an accurate phase screen using LCR-2500, its phase response curve is incorporated in the algorithm that writes the phase function to it. The measured phase shift for the LCR-2500 is plotted as a function of gray scale level (GSL) in Fig. 3. Its phase modulation is more than 2π at wavelength of 632.8nm. To obtain a phase-only modulation, there is only the polarization without an Analyzer in the experiment. Ideally, it will have no amplitude modulation for polarizer parallel to the liquid crystal director and without analyzer. The measured amplitude modulation is less than 10%.

Table 2. Specifications of LCR-2500

Parameters	Values
Active area dimensions	$19.5 \times 14.6 \text{ mm}^2$
Resolution	1024×768
Pixel pitch	$19 \mu\text{m} \times 19 \mu\text{m}$
Gray levels	256 (8 bit)
Frame rate	75 Hz
Reflectance	>75%
Cell gap	$5.5 \mu\text{m}$

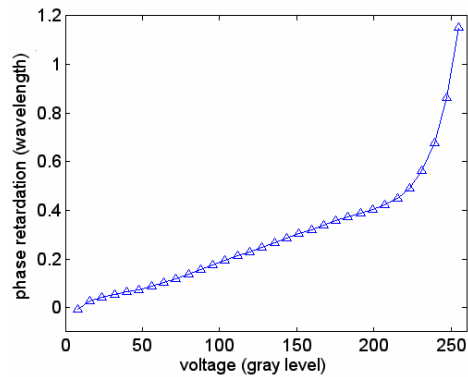


Fig. 3. Phase modulation for LCR-2500

The diagram of the experimental setup is shown in Fig. 4. After passing through polarizer, Laser from the He-Ne laser source becomes linear polarization. Then, it is focused by lens L1 and diffracted by pinhole H1 with the aperture of $20 \mu\text{m}$, which makes its power more homogeneously distributed. Then, after collimated by lens L2 with $f=300 \text{ mm}$ and reflected by LCR-2500, the Laser will be focused by lens L2, filtered by hole H2 with aperture of about 2 mm , and collimated by lens L3 with $f=10 \text{ mm}$. Finally, the HASO 32 can measure the wavefront of the incident laser. It should be noted that the HASO 32 works in relative

wavefront measurement mode in our experiment. And the reference wavefront is measured without a gray level distribution of turbulence on the LCR-2500. Therefore, the measured turbulence wavefronts will be close to simulated ones.

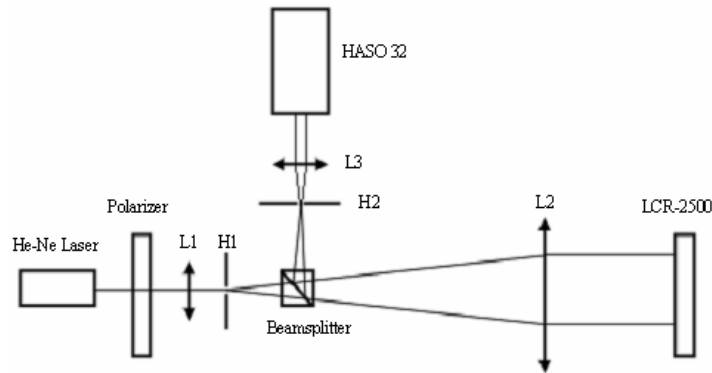


Fig. 4. Schematic diagram of the experimental setup, L1, L2 and L3: lens; H1 and H2: hole.

4. Results and discussion

As an example, we calculated the phase wavefront with R_z of 1m. Its size is relatively small. But it is enough to demonstrate the procedure to generate dynamic turbulence wavefronts. The diameter D of actual aperture of optical system is 0.6 m. Therefore, the physical size of turbulence wavefront corresponding to the LCOS is $0.8 \times 0.6 \text{ m}^2$, and its grid is 96×72 , which is a little less dense than that defined in table 1. The parameters used to simulate the turbulence wavefront are listed in table 3. For simplification, we select route B because only 4 wavefronts will be calculated. But for a long duration turbulence simulation, we should enlarge the size of R_z and select route A. The wind speed is 6m/s. And the refractive index structure constant at ground, $C_n^2(0)$, is $10^{-15} \text{ m}^{-2/3}$. The object distance is 300km above which the effects of turbulence could be ignored. The Monte Carlo analysis was conducted to evaluate the obtained turbulence wavefronts according to the phase structure function's 5/3 power. The obtained powers are shown in Fig. 5 for phase structure function of 1000 independent wavefronts corresponding to area with diameter of R_z . Their mean value is 1.56 that is very close to 5/3, which indicates that our results are very good and close to the Kolmogorov theory.

Table 3. Parameters used in the simulation

Parameter	Value
V	6 m/s
H	300 km
$C_n^2(0)$	$10^{-15} \text{ m}^{-2/3}$
zenith angle	0
r_0	0.10m
Number of Zernike modes	120
Lambda	$0.6328 \text{ } \mu\text{m}$
Simulated area	$1 \times 1 \text{ m}^2$
Sub-area	$0.8 \times 0.6 \text{ m}^2$
# of grid samples across sub-area (horiz/vert)	96×72
Duration	40 ms
Time step	10 ms

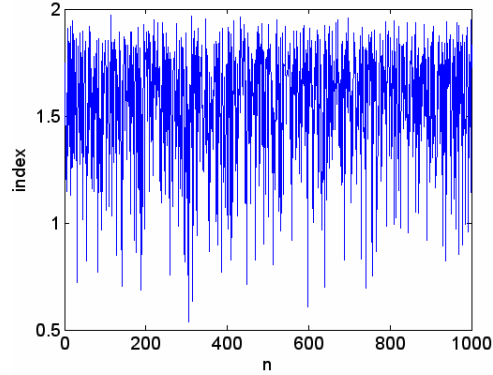


Fig. 5. Index of phase structure function for turbulence Monte Carlo simulation

And one of generated turbulence wavefronts with the phase structure function's power of 1.6595 is shown in Fig. 6. Because r_0 is about 0.10m according to Eq. (2) and the diameter of simulated area is 1m, the R_z/r_0 is 10. Therefore, to choose 120 Zernike modes is optimum in calculating speed and turbulence simulation precision according to our discussion in section 2. Pre-120 Zernike modes coefficients is used and also shown right in Fig. 6. It could be seen that tip and tilt aberrations dominate the turbulent wavefront, which accords with practical situations.

To produce the time-evolution wavefronts, the used calculation grid is 90×120 in a rectangle area inside the 1m diameter of simulated area that is the whole wavefront. We used a simulated area of $0.6 \times 0.8 \text{ m}^2$ with grid of 72×96 that is interpolated to for the LCOS. The time step between two neighbor wavefronts in calculation program is 10ms, that is, the next wavefront is sampled at a distance of wind speed 6m/s multiplied by 10ms away from our selected area, that is, 0.06m. Therefore, we simulated four phase screens along x axis with total time of 40ms and time step of 10ms. Then, the gray maps of the generated time-evolution turbulence wavefronts were calculated with the phase vs voltage (gray level) curve in Fig. 3. Then, they were sent to the LC screen. The turbulence wavefronts were measured with a wavefront sensor, HASO 32 of Imagine optic Ltd. Co. To minimize the effects of the aberration, φ_{LC} , of the LC screen, we measured it with a gray level of zero on the whole screen. Secondly, to minimize the diffractive effects of the regular pixel structure of the LC screen, we could introduce a tilt, φ_r , on the whole screen and filter the first order. Therefore, we could overcome their effects by calculating the gray level with sum of the turbulence wavefronts, φ , φ_{LC} and φ_r . As an example, the measured results of time series of 4 Kolmogorov turbulence wavefronts are shown in the Fig. 7. It should be noted that the pixilation in Fig. 6 corresponds to HASO 32 that is used to measure the wavefront. In the experiment, the L2 and L3 result that the area of LCOS is corresponding to a part of HASO 32's microlens 32×32 array due to compression effects of lens L2 and L3, the effective microlens array is 19×25 in the experiment.

It is really very important to produce the desired turbulence wavefront with LC devices. The wavefronts of low spatial frequency components are very similar the theoretical ones. But higher spatial frequency components could not be measured by the wavefront sensor. Its microlens array is 32×32 . And the used part in the paper is 19×25 . Therefore The wavefronts of higher spatial frequency components are not very similar because of small spatial sampling frequency of the wavefront sensor. However, LC wavefront corrector generates wavefront based on phase wrapping method. The phase wrapping level is 8. The diffractive wavefront at the first order should be the same as the theoretical one according to binary optics. In addition, unlike the deformable mirror, the LC device has no hysteresis phenomenon. Therefore, LC reproduces the turbulence profile reliably without mechanical movement.

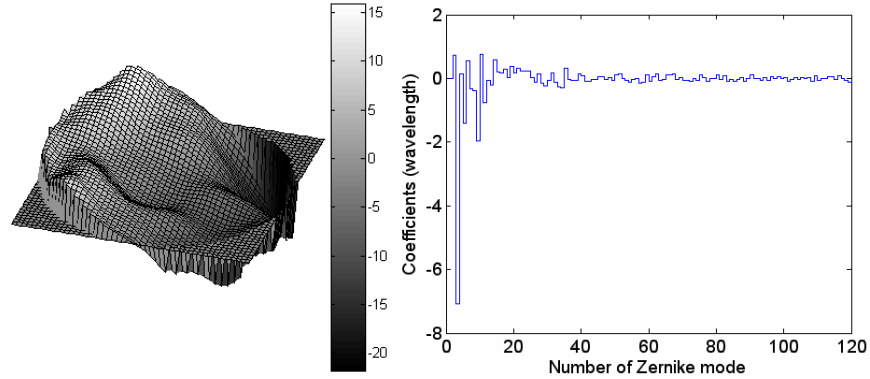


Fig. 6. Simulated turbulence wavefront in unit of wavelength (left) and correspondent pre-120 Zernike modes coefficients (right).

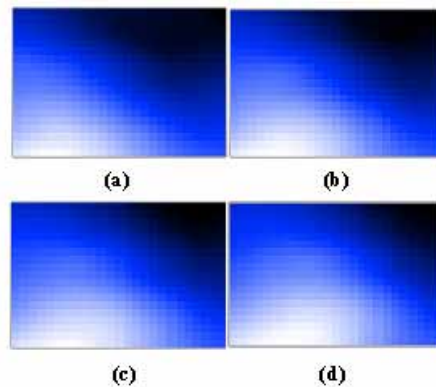


Fig. 7. Time series of 4 Kolmogorov turbulence wavefronts from left to right.

5. Conclusion

In summary, a procedure to calculate the time evolution turbulence wavefronts based on the covariance method is presented. First, parameters, such as wind speed, altitude and refractive index structure constant, are considered so as to obtain practicable results. Secondly, calculation speed was improved by optimizing the number of Zernike mode number and the mesh grid size. Thirdly, some factors about liquid crystal (LC) screen were taken into account to decrease the turbulence simulation error. Additionally, Taylor hypothesis is used to generate the time evolution wavefront. Finally, the time-evolution wavefronts disturbed by atmospheric turbulence generated by our LC atmospheric turbulence simulator (ATS) were measured with a wavefront sensor. And a programmable LC ATS based on Kolmogorov theory with the method is demonstrated.

Acknowledgments

Work was supported in part by grants from national nature science fund under the grants of National No. 60578035 and No. 50473040, and Science Foundation of Jilin Province under the grants of No. 20050520 and No. 20050321-2.